

RSC Advances



This is an *Accepted Manuscript*, which has been through the Royal Society of Chemistry peer review process and has been accepted for publication.

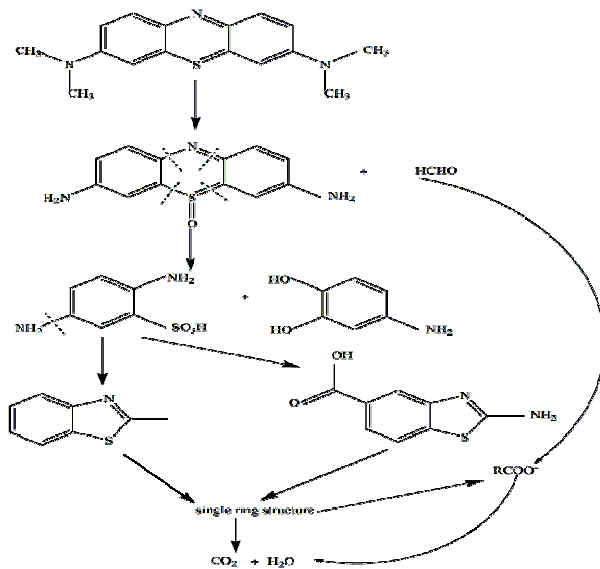
Accepted Manuscripts are published online shortly after acceptance, before technical editing, formatting and proof reading. Using this free service, authors can make their results available to the community, in citable form, before we publish the edited article. This *Accepted Manuscript* will be replaced by the edited, formatted and paginated article as soon as this is available.

You can find more information about *Accepted Manuscripts* in the [Information for Authors](#).

Please note that technical editing may introduce minor changes to the text and/or graphics, which may alter content. The journal's standard [Terms & Conditions](#) and the [Ethical guidelines](#) still apply. In no event shall the Royal Society of Chemistry be held responsible for any errors or omissions in this *Accepted Manuscript* or any consequences arising from the use of any information it contains.

Graphical abstract

The reduction degradation pathway of MB molecules



1

2 Reactivity of iron-based nanoparticles by green synthesis under
3 various atmospheres and their removal mechanism of methylene blue

4

5 Jiewen Lin¹, Xiulan Weng², Xiaoying Jin², Mallavarapu Megharaj³, Ravi Naidu³, Zuliang
6 Chen^{2,3*}

7 1. School of Chemistry and Chemical Engineering, Fujian Normal University, Fuzhou 350007,
8 Fujian Province, China

9 2. School of Environmental Science and Engineering, Fujian Normal University, Fuzhou
10 350007, Fujian Province, China

11 3. Global Centre for Environmental Remediation, University of Newcastle, Callaghan NSW
12 2308, Australia

13 *Corresponding author. Ph: 61-02-49139748; Email: Zuliang.chen@newcastle.edu.au

14

15

16

17

18

19

20

21

22

Abstract

In this study, iron-based nanoparticles (Fe NPs) were synthesized using tea extracts under various atmospheres (N₂, O₂ and air) to understand how atmospheres impacting on the reactivity of Fe NPs, where Fe NPs were used for the degradation of methylene blue (MB). SEM and FTIR confirmed the morphology and change in size of iron-based nanoparticles before and after reaction with MB, indicating that different Fe composition, morphology and size were obtained under various atmospheres then resulted in different reactivity of Fe NPs. In addition, various parameters impacting on removing MB by Fe NPs synthesized under various atmospheres show that the solution pH significantly affecting the reactivity of Fe NPs. Furthermore, the dates fitted well to the pseudo-second-order adsorption and pseudo-first-order reduction models, confirming that the removing MB based on both adsorption and reduction. Langmuir and Freundlich isotherms demonstrate that the removal of MB by Fe NPs synthesized under various atmospheres was different due to their composition, morphology and size. Finally, the degraded products such as benzothiazole were identified by Gas chromatography-mass spectrometry (GC-MS) after the degradation of MB, and finally a feasible removal pathway is proposed.

39

Keywords: Fe NPs; Atmosphere; Green synthesis; Methylene Blue.

41

42

43

44

45

46

47

48 1. Introduction

49 Dyes are generally used in textiles, paper, tanneries and rubber manufacturing, and removing
50 dye from discharge effluents remains a serious problem ^[1]. The dyes such as Methylene blue
51 (MB) releasing into the environment may cause an increase in chemical and biological
52 oxygen demand, and it is difficult to be decomposed by microbes ^[2]. Since MB is a type of
53 cationic dye with a great stability, resulting in the degradation of MB by the methods such as
54 biological, chemical precipitation and adsorption is difficult ^[3]. Activated carbon ^[4] and wheat
55 shells were used to remove basic dye from aqueous solutions ^[3].

56

57 Developments in nanotechnology have allowed iron nanoparticles (Fe NPs) to be the subject
58 of increasing attention in the field of wastewater treatment containing dyes. The mechanisms
59 for removing dyes and their dependence on adsorption and reduction by Fe NPs have been
60 proposed. For instance, magnetic Fe₃O₄ nanoparticles were utilized for adsorption of neutral
61 red dye from aqueous solution ^[4]. Nanoscale zero-valent iron (nZVI) supported bentonite was
62 used to degrade acid violet red B ^[5]. To date, numerous methods have been developed for the
63 synthesis of Fe NPs, and the chemical method of using sodium borohydride (NaBH₄) as a
64 reducing agent is often employed in the synthesis of Fe NPs. Drawbacks in the chemical
65 method include low production rates, high energy consumption, and high cost, as well as
66 contamination arising from chemical precursors, toxicity of the used solvents and generation
67 of hazardous by-products ^[6, 7]. In contrast, the green synthesis of metal nanoparticles using
68 plant extracts due to the ability of polyphenols to function as natural reducing agents has been
69 proposed as an alternative to the chemical method ^[7]. Hence, synthesis of metal nanoparticles
70 using plant extracts is generally cost-effective, biocompatible, non-toxic, and eco-friendly ^[6, 7].

71

72 In developing the green synthesis of Fe NPs, only a few studies have been done using plant
73 extracts for synthesis of Fe NPs. Consequently, there are limitations in understanding the
74 effect of synthetic conditions on the morphology and size distribution of Fe NPs, which
75 involve the reactivity of FeNPs. In this paper, iron-based nanoparticles synthesized by green
76 tea extracts passing N₂, O₂ and air and their used for the removal of MB in aqueous solution
77 were investigated. In addition, we particularly investigate the mechanism for removing MB
78 using kinetic studies. Thus, the following aspects were done: (1) characterization of Fe NPs
79 synthesized under N₂ (N-Fe NPs), O₂ (O-Fe NPs) and air (air-Fe NPs) before and after
80 reaction with MB to understand their differences in morphology and size, (2) the reactivity of
81 Fe NPs synthesized under N₂, O₂ and air by estimation of various experimental parameters
82 affecting the removal of MB; (3) the study of adsorption and reduction kinetics to further
83 understand the removal process of MB and proposing a feasible removal mechanism.

84

85 **2. Experimental**

86 *2.1. Preparation of Fe NPs (N₂, O₂ and air)*

87 The extract of green tea was prepared by adding 60 g of processed green tea leaf into 1000
88 mL distilled water in a water bath heated at 353K for 1 h. Then the extracts were taken for
89 vacuum filtration after cooling to room temperature. Before 0.10 mol/L Fe₂SO₄ was added to
90 the tea extracts with a ratio volume of 1:2, we passed it into the N₂, O₂ or air and kept it in a
91 ventilation state during the synthetic process. Following vacuum-filtration this mixture's
92 complete reaction was taken to the vacuum drying chamber for 12 h. Only then were these
93 nano-solid particles used to remove MB.

94

95 *2.2. Characterization*

96 Scanning electron microscopy (SEM) images of GT-Fe NPs synthesized under N₂, O₂ and air

97 before and after reaction with MB were acquired using a JSM-7500F (JEOL Ltd. Co., Tokyo,
98 Japan) to observe the surface morphology and size. The spectrum of MB, green tea extract,
99 and Fe NPs inletting N₂, O₂ and air before and after reaction with MB were determined by
100 Fourier transform infrared spectroscopy (FTIR Nicolet 5700, Thermo Corp., USA). A 1%
101 specimen was mixed with 100 mg KBr to press into a sheer slice so that any changes in the
102 functional groups before and after reaction could be observed.

103

104 The MB degradation products were characterized by Gas chromatography-mass spectrometry
105 (GC-MS, Thermo Corp., USA). The analytical conditions are listed as follows: ethyl acetate
106 as solvent; capillary column (30 mm) as separation; helium as carrier gas and the sample
107 volume set at 270 °C. The temperature programs were determined since the initial temperature
108 was 50 °C for 2 min and then programmed to increase by 30°C per minute up to 220 °C and
109 then hold at 220 °C for 3 min. Then temperature was increased up to 260 °C by 6 °C per
110 minute for 10 min holding. The mass spectrometry starts from 20 to 600 (m/z).

111

112 *2.3. Batch experiments*

113 To compare the removal efficiency of MB in aqueous solution, the degradation experiments
114 were carried out using Fe NPs (0.03 g) synthesized under N₂, O₂ and air synthesized added to
115 30 mL MB at diverse conditions. Mixed solutions were stirred on a rotary shaker (125 rpm) at
116 298K to various time intervals, then centrifuged at 7000 rpm for 5 min. The influence of
117 experiment parameters on the removing MB was investigated. For instance, dosage of Fe NPs
118 was 0.5-2 g L⁻¹ in this study, initial concentration of MB was 50-100 mg L⁻¹, the reaction
119 temperature was 298-313K, and solutions of pH values ranged from 3.03-9.44. Experiments
120 were carried out in duplicate. The removal efficiency of MB using N-Fe NPs, O-Fe NPs and

121 air-Fe NPs vs the time (5, 10, 20, 30, 40, and 50 min) at the temperature of 293K, 298K,
122 303K and 313K, respectively were showed in Fig. S1. The various kinetic parameters were
123 obtained from fitting the concentration of MB vs the time. To investigate the stability of the
124 Fe NPs, the recyclable experiments were conducted at the optimum condition of T=313K,
125 $C_0=50 \text{ mg L}^{-1}$, $C=1 \text{ g L}^{-1}$ and pH=9.44 for three times, and the results were showed in Fig. S2.
126 UV-visible Spectrophotometer (722 N, Shanghai, China) was used to detect the concentration
127 of MB solution at $\lambda_{max}= 665 \text{ nm}$ (Fig. S3). The efficiency in removing MB was calculated
128 using the following equation [6].

$$129 \quad \eta = \frac{C_0 - C_t}{C_0} \quad (1)$$

130 Where η (%) represents the MB removal percentage, and C_0 and C_t (mg L^{-1}) represent the
131 concentration of MB at initial and t time, respectively.

132

133 3. Results and discussion

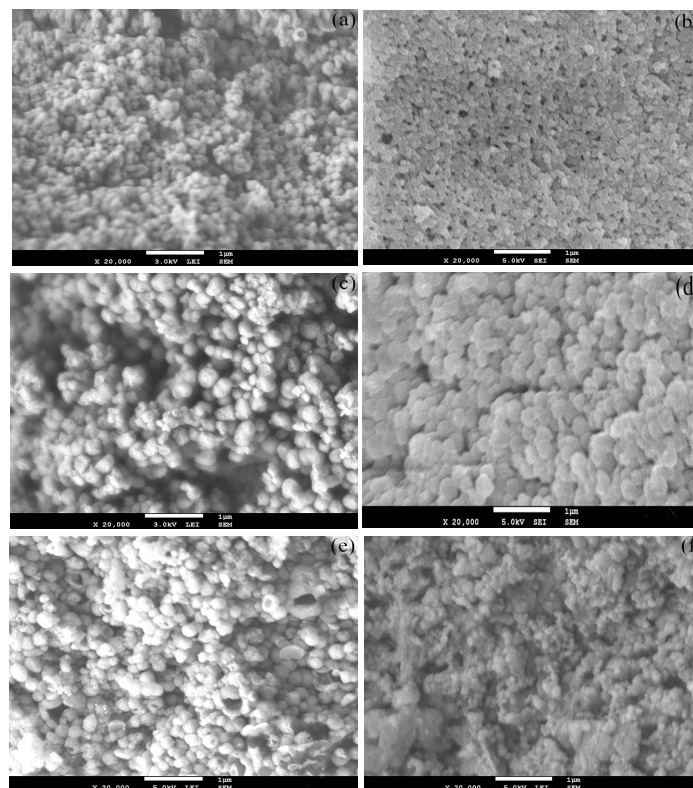
134 3.1 Characterization

135 3.1.1 SEM analysis

136 The morphology and size of N-Fe NPs, O-Fe NPs and air-Fe NPs are observed in Fig. 1. The
137 images of in Fig. 1 (a), (c) and (e) show Fe NPs (N_2 , O_2 and air) before reaction with MB,
138 respectively, which confirm that the Fe NPs have a spheroid morphology. The size of N-Fe
139 NPs, O-Fe NPs and air-Fe NPs is 87.4, 141.2 and 117.8 nm, respectively. This is because it is
140 difficult to oxidize Fe^0 in N_2 atmosphere hence the sizes of N-Fe NPs are smallest which
141 agrees with the following analysis of FTIR. Additionally, the images of in Fig. 1 (b), (d) and
142 (f) present Fe NPs (N_2 , O_2 and air) after reaction with MB. It can be observed that the surface
143 of Fe NPs became scabrous when they gathered into clusters and the sizes of N-Fe NPs, O-Fe

144 NPs and air-Fe NPs were determined as being 131.9, 271.2 and 182.4 nm, respectively. This
145 is due to: (1) iron oxide and hydroxide (Fe_3O_4 , Fe_2O_3 , $\text{Fe}(\text{OH})_3$ and $\text{Fe}(\text{OOH})$) forming on
146 the surface of Fe NPs after their reaction with MB^[8]; and (2) MB molecules or degraded
147 products were adsorbed onto the Fe NPs' surface.

148



149

150 **Fig. 1** SEM images of N-Fe NPs before (a) and after (b) reaction with MB; O-Fe NPs before
151 (c) and after (d) reaction with MB; air-Fe NPs before (e) and after (f) reaction with MB

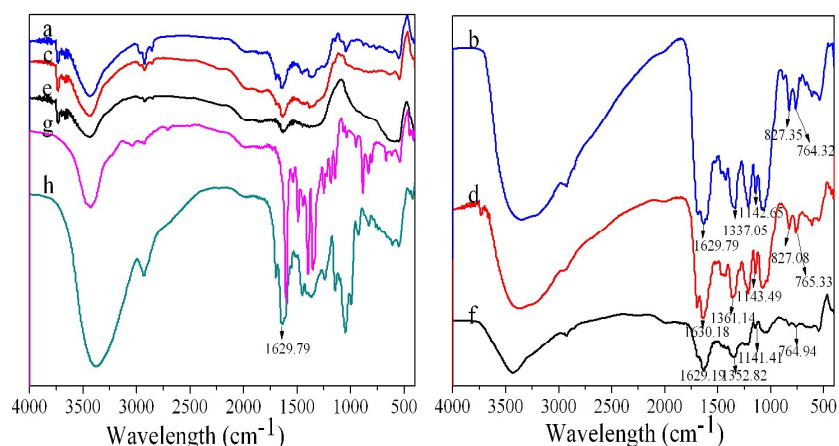
152

153 3.1.2 FTIR analysis

154 The results of FTIR are shown in Fig. 2, which represent Fe NPs (N_2 , O_2 and air) before and
155 after reaction with MB, green tea extract and MB powder. As shown in Fig. 2(a), (c) and (e),
156 the bands around 1629 cm^{-1} , which are attributed to the stretching vibration of the C=C
157 groups of organics of green tea extract, reflect the higher carbohydrate content of all the fresh

158 Fe NPs. The band at approximately 1337 cm^{-1} corresponds to the asymmetric vibration of the
 159 $\text{C}_{\text{Ar}}\text{-N-CH}_3$ ^[9] and the band at approximately 765 cm^{-1} corresponds to the Fe-OH vibration.
 160 Compared to the FTIR spectra for fresh Fe NPs (Fig. 2 (a), (c) and (e)), change in bands from
 161 used Fe NPs is observed in Fig. 2(b), (d) and (f). As shown in Fig. 2(b), (d) and (f), the bands
 162 at around 827 cm^{-1} correspond to the =C-H plane bending vibration on benzene which were
 163 also detected in Fig 2(h), indicating that the MB molecules were adsorbed onto the surface of
 164 Fe NPs (N-Fe NPs, O-Fe NPs and air-Fe NPs)^[9].

165



166

167 **Fig. 2** FTIR spectra of N-Fe NPs before (a) and after (b) reaction with MB; O-Fe NPs by pass
 168 before (c) and after (d) reaction with MB; air-Fe NPs by before (e) and after (f) reaction with
 169 MB; green tea extract (g); MB powder (h)

170

171 There were strong bands at $1337\text{-}1361\text{ cm}^{-1}$ referring to $\text{C}_{\text{Ar}}\text{-N}$ (stretching between aromatic
 172 ring and nitrogen atom) and CH_3 asymmetric vibration, the N- CH_3 stretching at 1143 cm^{-1} .
 173 These were all attributable to MB or its degraded products. The bands at approximately 764
 174 cm^{-1} were C-H out of plane bending vibration on benzene, which probably corresponded to
 175 the degraded products of MB by Fe NPs. The adsorption band at 1630 cm^{-1} signified the C=C
 176 stretching vibration ^[9] and was shifted subtly to broadly imply that MB was most likely

177 adsorbed onto the surface of Fe NPs (N₂, O₂ and air).

178

179 When comparing the differences in Fig. 2(b), (d) and (f), which represents the degradation of
180 MB by N-Fe NPs, O-Fe NPs and air-Fe NPs, respectively, the wavelength of various
181 functional groups shifting to longer wavelength on O-Fe NPs is observed. However, the high
182 band intensity indicates that the MB molecules are adsorbed onto the surface of Fe NPs, yet
183 on the other hand, the degraded products reduced by Fe NPs are capped simultaneously on the
184 surface ^[7, 8]. Additionally, it emerged that the intensity of band corresponded to N-Fe NPs
185 more strongly than the O-Fe NPs and air-Fe NPs. This is due to the fact that the MB
186 molecules on the surface of N-Fe NPs were reduced by Fe⁰, resulting in the surface active
187 sites being unsaturated and more MB molecules adsorbed. The mentioned above results from
188 FTIR provide the evidence for the removal of MB based on the both adsorption and reduction
189 ^[8].

190

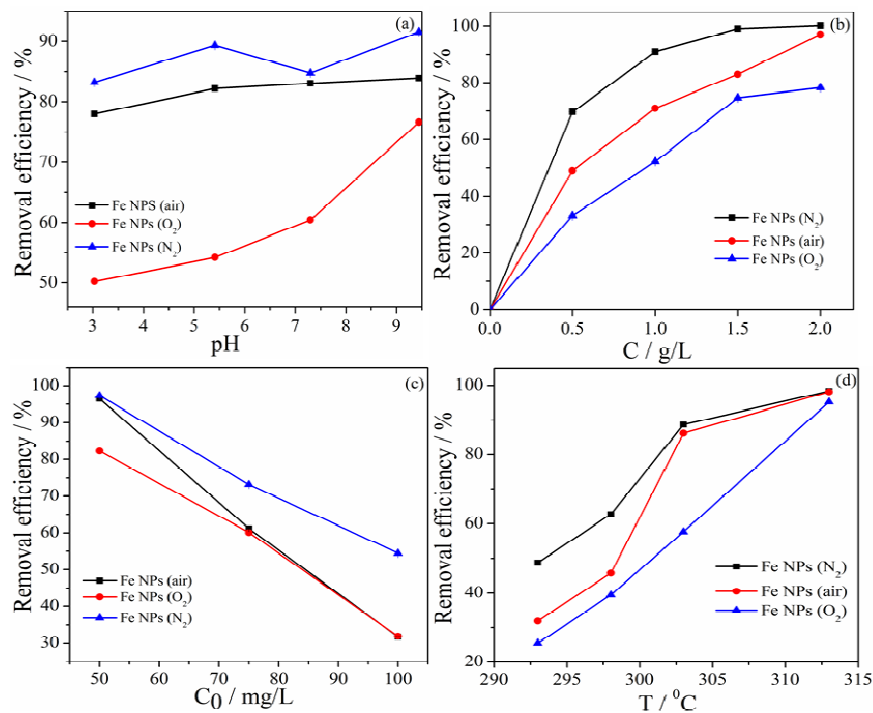
191 *3.2 The effect of various parameters on removing MB*

192 *3.2.1 Effect of initial pH values*

193 The initial pH value is one of the most significant parameters influencing the removal process
194 of dyes for water treatment since the charge of surface on adsorbent and dye molecules can be
195 influenced by pH values in aqueous solution ^[10, 11]. As shown in Fig.3 (a), the efficiency in
196 removing MB by N-Fe NPs, O-Fe NPs and air-Fe NPs was improved when the pH range
197 increased from 3.03 to 9.44. This is due to the surface active sites of Fe NPs (N₂, O₂ and air)
198 transforming from positive to negative charge when pH increased, resulting in the presence of
199 electrostatic attraction between the adsorbents and MB molecules since MB molecule is
200 intrinsically cationic dyes. In contrast, Fe⁰ can be corroded to form maghemite (γ -Fe₂O₃),
201 magnetite (Fe₃O₄) and iron hydroxides ^[6]. On the other hand, we can conclude that the effect

202 of removing MB by N-Fe NPs (91.5%) was better than that of O-Fe NPs (76.6%) and air-Fe
 203 NPs (83.9%) at pH=9.44. This is due to the fact that Fe⁰ occupying most of the internal
 204 structure of N-Fe NPs while iron oxide nanoparticles occupied the main parts of the surface of
 205 both O-Fe NPs and air-Fe NPs.

206



207

208 **Fig. 3.** Degradation of MB at experiment parameters. (a) Effect of the initial pH values.
 209 Condition: 1.0 g L⁻¹; 50 mg L⁻¹; 30 mL; 298K; 125 r min⁻¹; (b) Effect of dosages of Fe NPs
 210 (N₂, O₂ and air). Condition: pH = 7.3; 50 mg L⁻¹; 30 mL; 298K; 125 r min⁻¹; (c) Effect of
 211 initial concentration of MB. Condition: pH = 7.3; 1.0 g L⁻¹; 30 mL; 298K; 125 r min⁻¹; (d)
 212 Effect of temperature. Condition: pH = 7.3; 1.0 g L⁻¹; 30 mL; 50 mg L⁻¹; 125 r min⁻¹

213

214 3.2.2 Effect of dosage of Fe NPs

215 The effect of Fe NPs dosage on the removal of MB via Fe NPs (N₂, O₂ and air) is presented in
 216 Fig. 3 (b), where we can observe that increasing the amount of adsorbent (range from 0.5-2.0

217 g L⁻¹) enhanced the dye removal efficiency. This is attributed to the larger iron surface area
218 and more available adsorption active sites^[10]. Moreover, the adsorption capacity of Fe NPs
219 increases when the adsorbent dosage also increases. As shown in Fig. 3 (b), when the amount
220 of adsorbent increases to 2.0 g L⁻¹, the removal efficiency of MB using Fe NPs (N₂, air and O₂)
221 reach 100.0%, 97.0% and 78.2% respectively. It can be seen that the N-Fe NPs were the
222 most efficient in removing MB compared to the others, contributing to the presence of zero-
223 valent iron nanoparticles. Moreover this finding is consistent with the above conclusion.

224

225 3.2.3 Effect of initial concentration of MB

226 The effect of initial dye concentration in solution on the efficiency in removing MB is
227 documented in Fig. 3 (c). As the initial MB concentration increases from 50 to 100 mg L⁻¹,
228 the percentage of MB removed by N-Fe NPs declines from 97.4% to 55.6%, while that by O-
229 Fe NPs slowing down markedly from 83.0% to 32.5% and that by air-Fe NPs is between them.
230 The removal efficiency of dye decreased when dye concentration increased, because there
231 were less available surface active sites for constant adsorbent dosage. Furthermore, mass-
232 transfer resistance inhibited MB molecules being adsorbed onto the surface of Fe NPs from
233 solution phase^[11]. However, the presence of Fe⁰ in N-Fe NPs led to the difference with O-Fe
234 NPs and air-Fe NPs in terms of efficiently removing MB. Therefore we can conclude that N-
235 Fe NPs are the most efficient in removing MB.

236

237 3.2.4 Effect of temperature

238 Temperature plays an important role in influencing the removal efficiency of adsorption and
239 reduction process for MB by Fe NPs (N₂, O₂ and air). The effect of reaction temperature
240 (293K, 298K, 303K and 313K) on the removal efficiency using Fe NPs is depicted in Fig. 3
241 (d). Here, the efficiency of N-Fe NPs in removing MB was 51.4, 87.3, 89.4 and 98.4%, at

242 temperatures of 298, 293, 303 and 313K, respectively. It is indicated that the removal of MB
243 by N-Fe NPs was an endothermic process. However, as shown in Fig. 3 (d), the removal
244 efficiency of MB by O-Fe NPs was 25.4, 39.5, 57.7, and 95.2% at temperatures of 293, 298,
245 303 and 313K, respectively. It is suggested that the O-Fe NPs were less efficient in removing
246 MB compared to N-Fe NPs because the surface of O-Fe NPs was covered with iron oxide and
247 hydroxide. Meanwhile, the air-Fe NPs' efficiency when removing MB was determined by the
248 amount of nZVI and iron oxide nanoparticles these particles contained. Consequently, the
249 efficiency in removing dyes can be boosted by raising the temperature because this serves to
250 encourage collisions between MB molecules, which in turn lead to more activation energy [12].
251 Homologous phenomena have been reported in some studies [10, 13]. Moreover, this result
252 agrees with the kinetic study which is reported below.

253

254 3.3 Kinetic study

255 Previous reports [14, 15] have indicated that MB removal by Fe NPs involves adsorption and
256 reduction. However, to further confirm the removal of MB based on adsorption and reduction,
257 adsorption and reduction kinetics, adsorption isotherms and thermodynamic models were
258 used to fit the data. The amount of absorbed MB was calculated using the following formula
259 [15, 16].

$$260 \quad q_e = \frac{(C_i - C_e)V}{m} \quad (2)$$

261

262 where q_e (mg g^{-1}) represents the amount of MB absorbed by Fe NPs at equilibrium, C_i (mg L^{-1})
263 1), the concentration of MB in solution at time t , C_e (mg L^{-1}), the equilibrium concentration of
264 MB in solution, V (mL), the volume of MB solution used and m (g) is the weight of the
265 adsorbent used.

266 3.3.1 Adsorption kinetics

267 The adsorption of MB onto Fe NPs synthesized under various atmospheres may involve
268 physical and chemical sorption. The dynamic process of MB adsorption was analyzed by
269 using pseudo-first-order and pseudo-second-order equations, because these kinetic models are
270 often applied to fit the process of adsorption. Pseudo-first-order equation is described as
271 follows [17]:

272
$$\ln(q_e - q_t) = \ln q_e - k_1 t \quad (3)$$

273
274 where q_e (mg g^{-1}) is the number of MB molecules absorbed onto the absorbent at equilibrium,
275 q_t (mg g^{-1}) is the amount absorbed at time t and k_1 (min^{-1}) is the rate constant of pseudo-first-
276 order adsorption that can be calculated from the slope of linear plot of $\ln(q_e - q_t)$ versus t .

277 The linear kinetic equation of pseudo-second-order can be given as follows [17]:

278
$$\frac{t}{q_t} = \frac{1}{k_{ps} q_e^2} + \frac{t}{q_e} \quad (4)$$

279 where q_e and q_t (mg g^{-1}) correspond to adsorption capacities at equilibrium and time,
280 respectively; and k_{ps} ($\text{g mg}^{-1} \text{min}^{-1}$) is the rate constant of pseudo-second-order adsorption
281 equation that can be obtained by calculating the intercept of the linear equation.

282

283 The kinetic parameters, correlation coefficients (r^2) and rate constant (k), of pseudo-first-order
284 and pseudo-second-order models, were calculated from equations (3) and (4). As shown in
285 Table 1, the r^2 was more than 0.896 which indicated that the adsorption of MB by N-Fe NPs,
286 O-Fe NPs and air-Fe NPs all suited the pseudo-second-order model. Compared to the pseudo-
287 first-order model, the coefficient values for the pseudo-second-order model ranged from 0.89-
288 1.00 for the N-Fe NPs. This indicated that the sorption process mainly involved

289 chemisorption. Meanwhile the rate constant also rose as T increased (the range of k_2 was 0.03-
 290 48.24), implying the adsorption of MB may be an endothermic process, which further proved
 291 that temperature had a significant impact on the rate constant. The correlation coefficients (r^2)
 292 of pseudo-first-order in the range from 0.45-0.97 for O-Fe NPs, were less than that of pseudo-
 293 second-order (the range of r^2 was 0.98-0.99), confirming that the sorption of MB onto O-Fe
 294 NPs fitted well with to the pseudo-second-order model.

295

296 **Table 1** Adsorption kinetics parameters for the removal of MB by Fe NPs (N_2 / O_2 / air)

N_2				
Temp (K)	Pseudo-first-order model		Pseudo-second-order	
	k_1 (min^{-1})	r^2	k_2 ($\text{g mg P}^{-1} \text{min}^{-1}$)	r^2
293	0.2055	0.7759	0.0261	0.8961
298	0.0598	0.8900	1.8029	0.9987
303	-0.0261	0.4054	0.8343	0.9997
313	0.0041	0.0100	48.3139	1.0000
O_2				
Temp (K)	Pseudo-first-order model		Pseudo-second-order	
	k_1 (min^{-1})	r^2	k_2 ($\text{g mg P}^{-1} \text{min}^{-1}$)	r^2
293	0.0521	0.4515	0.2584	0.9836
298	0.0859	0.8493	0.1751	0.9876
303	0.1003	0.8871	0.0462	0.9879
313	0.0527	0.9751	0.0721	0.9990
air				
Temp (K)	Pseudo-first-order		Pseudo-second-order	
	k_1 (min^{-1})	r^2	k_2 ($\text{g mg P}^{-1} \text{min}^{-1}$)	r^2
293	0.0464	0.94	0.6589	0.9988
298	0.0360	0.9012	0.9546	0.999
303	0.0299	0.8317	0.1479	0.9588
313	0.0949	0.952	1.4292	1.0000

297

298 However, the pseudo-first-order model can be also used to describe the adsorption process
 299 with O-Fe NPs comparing to N-Fe NPs at 313K, implying the adsorption capacity of O-Fe
 300 NPs was stronger due to the contents of iron oxide nanoparticles. Furthermore, the adsorption
 301 capacity of air-Fe NPs may lie between N-Fe NPs and O-Fe NPs, which will be further
 302 proven by Langmuir isotherms models. The adsorption process of MB by various adsorbents
 303 has been reported previously ^[11, 17] Furthermore all the experimental data showed that the

304 adsorption process of MB fitted well to the pseudo-second-order model, and it occurred
305 through chemisorption rather than physical adsorption.

306

307 3.3.2 Reduction kinetics

308 The process of removing MB by Fe NP (N₂, O₂ and air) includes not only chemical
309 adsorption, but may also involve chemical reaction. Therefore, reduction kinetics was
310 investigated to further understand the removal process. Pseudo-first-order and pseudo-second-
311 order models were provided as shown below ^[18]:

$$312 \quad \ln \frac{C}{C_0} = -k_{obs}t \quad (5)$$

$$313 \quad \ln \left(\frac{1}{C_t} - \frac{1}{C_0} \right) = kt \quad (6)$$

314 where k_{obs} and k correspond to the pseudo-first and pseudo-second-order rate constants,
315 respectively. C_0 and C_t present the initial and instantaneous concentration of MB in aqueous
316 solution at $t=0$ and $t=t$.

317

318 As shown in Table 2, with reference to the N-Fe NPs, values of the regression coefficients (r^2)
319 of the pseudo-second-order model ranged from 0.8583 to 0.8971. However, the pseudo-first-
320 order model indicated that regression coefficients (r^2) ranged from 0.7589 to 0.9252,
321 illustrating the reduction process of MB fitted well to pseudo-first-order kinetics. Associated
322 with the above finding, it can be concluded that the process of removing MB by N-Fe NPs
323 may involve chemical reaction, due to there being much more zero-valent iron nanoparticles
324 (nZVI) in N-Fe NPs than in O-Fe NPs, where the degraded products was proven by GC-MS
325 analysis. Values of the regression coefficients (r^2) of O-Fe NPs are demonstrated in Table 2.
326 They range from 0.7468 to 0.9735 in the pseudo-first-order kinetic model and 0.9382 to

327 0.9703 for the pseudo-second-order kinetic model. It indicates that the pseudo-second-order
328 model can describe the kinetic process more properly.

329

330 **Table 2** Reduction kinetics parameters for the removal of MB by Fe NPs (N₂/ O₂/ air)

N ₂				
Temp (K)	Pseudo-first-order		Pseudo-second-order	
	k ₁ (min ⁻¹)	r ²	k ₂ (g mg P ⁻¹ min ⁻¹)	r ²
293	0.0085	0.7589	0.0035	0.8732
298	0.0052	0.9039	0.0024	0.9179
303	0.0058	0.8775	0.0105	0.8583
313	0.0063	0.9252	0.0636	0.8971
O ₂				
Temp (K)	Pseudo-first-order		Pseudo-second-order	
	k ₁ (min ⁻¹)	r ²	k ₂ (g mg P ⁻¹ min ⁻¹)	r ²
293	0.0027	0.7468	0.0006	0.7371
298	0.0037	0.9174	0.0013	0.9576
303	0.0107	0.9563	0.004	0.9668
313	0.0405	0.9735	0.0424	0.9703
air				
Temp (K)	Pseudo-first-order		Pseudo-second-order	
	k ₁ (min ⁻¹)	r ²	k ₂ (g mg P ⁻¹ min ⁻¹)	r ²
293	0.0014	0.9426	0.0004	0.9463
298	0.0015	0.9685	0.0005	0.9670
303	0.0243	0.8706	0.0188	0.7742
313	0.0404	0.8668	0.1960	0.9617

331

332 The removal of MB by O-Fe NPs was a more complicated process, as proven by SEM, there
333 was a thick layer of iron oxide nanoparticles on the surface of O-Fe NP. Firstly, the MB
334 molecules were transferred from liquid to solid via electrostatic interaction and π - π
335 interaction of species groups between adsorbate-adsorbent [19]. Then, MB molecules were
336 adsorbed into the interface of O-Fe NPs due to the presence of adsorption sites. Lastly,
337 adsorbed molecules that made contact with nZVI were then reduced by O-Fe NPs.
338 Nevertheless, the restored strength was relatively weak because there was little nZVI content.
339 Consequently, the results for reduction kinetics demonstrated that the degradation of MB by
340 N-Fe NPs was more efficient than that of O-Fe NPs and air-Fe NPs.

341

342 3.4 Adsorption isotherms

343 To further analyze the process of adsorption, the Langmuir and Freundlich isotherm models
344 were employed to fit the experimental data. The Langmuir adsorption isotherm assumes that
345 adsorbents' surface sites are homogeneous and the adsorption process is a monolayer
346 adsorption. It has been successfully used for describing the dynamic process of adsorption.
347 The linear equation of the Langmuir model is given as follows ^[20]:

$$348 \quad \frac{C_e}{q_e} = \frac{1}{q_{\max} K_L} + \frac{C_e}{q_{\max}} \quad (7)$$

349
350 where C_e (mg L^{-1}) is the equilibrium concentration of MB solution; q_e (mg g^{-1}) represents the
351 amount adsorbed at equilibrium; q_{\max} (mg g^{-1}); and K_L (L mg^{-1}) corresponds to the maximum
352 adsorption capacity and the Langmuir constant or equilibrium constant that can be calculated
353 from the slope and intercept of the linear regression C_0/q_e versus C_e .

354
355 The linear equation of the Freundlich isotherm, which is an empirical formula and describes
356 the adsorption that takes place on the heterogeneous surface of an adsorbent, can be shown as
357 follows ^[20]:

$$358 \quad \log q_e = \log K_F + \frac{1}{n} \log C_e \quad (8)$$

359 where C_e and q_e represent the equilibrium concentration of MB in aqueous solution and the
360 equilibrium adsorbed. K_F and $1/n$ are the Freundlich constants, which relate to adsorption
361 capacity and adsorption intensity, respectively. K_F was generally used to describe the strength
362 of the relationship between adsorbate and adsorbent ^[21]. The values of n in the 1 to 10 range
363 represent good adsorption, indicating that this process favored adsorption.

364

365 All the parameters values are summarized in Table 3 in terms of Eqs. (7) and (8). The
 366 adsorption isotherm is critical for investigating the adsorption system, which describes the
 367 correlation between adsorbate and adsorbent. As shown in Table 3, the r^2 values were all
 368 higher than 0.99, indicating the adsorption of MB by N-Fe NPs and O-Fe NPs fitted well to
 369 the Langmuir isotherm equation. The values illustrated that the N-Fe NPs or O-Fe NPs'
 370 adsorption of MB was a monolayer process due to the homogeneous active sites on the
 371 surface of Fe NPs. The Langmuir adsorption isotherm equation hypothesized that the
 372 adsorbents' surface active sites were homogeneous and had identical energy. Furthermore the
 373 active sites were saturated when monolayer molecules were adsorbed onto the adsorbent
 374 surface. The maximum adsorption capacity q_{\max} for MB onto N-Fe NPs and O-Fe NPs was
 375 obtained from the slope of the linear equation and the values shown in Table 3 were 52.910
 376 and 28.329, respectively. Thus the adsorption strength of N-Fe NPs for MB was higher than
 377 O-Fe NPs due to reduction of NZVI. The Freundlich exponents ($r^2 = 0.3897$ and 0.2131 ,
 378 respectively) were less than that of Langmuir, confirming that the Freundlich adsorption
 379 isotherms model did not properly fit the MB adsorption process.

380

381 **Table 3** Isotherm parameters for the removal of MB by Fe NPs (N₂/ O₂/ air)

Parameters	Langmuir			Freundlich			
	q_{\max} (mg g ⁻¹)	K_L (L mg ⁻¹)	r^2	K_f (L mg ⁻¹)	n (g L ⁻¹)	r^2	R_L
N ₂	52.9100	0.7975	0.9931	45.5407	37.4531	0.3897	0.03-0.31
O ₂	28.3286	0.2822	0.9908	37.2992	-21.367	0.2131	0.05-0.16
air	28.7356	0.3207	0.9906	56.5588	-6.8540	0.9613	0.04-0.46

382

383 The values of dimensionless constant separation factor (R_L) can be calculated using the
 384 following equation ^[21], which is another essential parameter of the Langmuir isotherm:

385

$$R_L = \frac{1}{(1 + bC_i)} \quad (9)$$

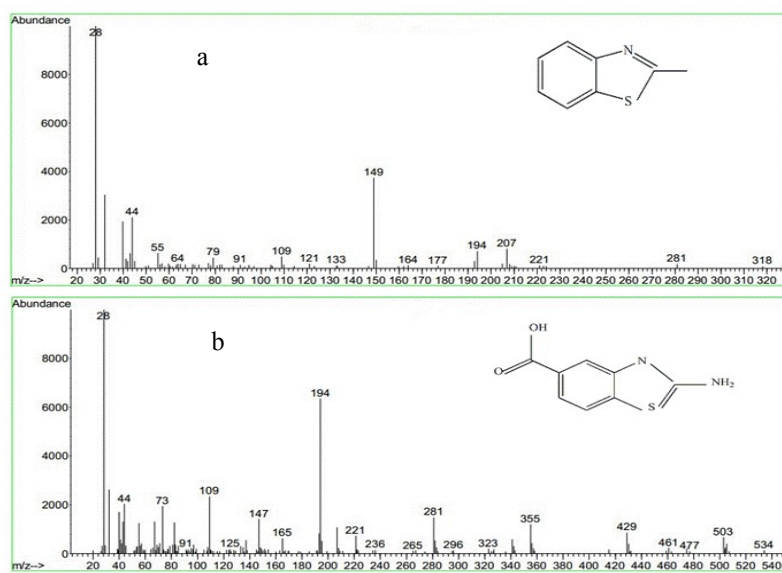
386 The results of R_L given in Table 3 were $1 > R_L > 0$ for the adsorption of MB onto N-Fe NPs (in
387 the 0.03-0.31 range) and O-Fe NPs (in the 0.05-0.16 range), demonstrating the adsorption
388 process for MB was favorable [22].

389

390 3.6 Degraded products analysis

391 The degradation products of MB using Fe NPs (N_2 , O_2 and air) were conducted by GC-MS
392 analysis, and the results were shown in Fig. 4 (a) and (b), respectively. A possible degradation
393 pathway of MB using Fe NPs is illustrated in Fig. 5. Analogues of benzothiazole were
394 detected in the degradation, a phenomenon that has been documented previously [23, 24]. As
395 shown in Fig. 4, the signals at $m/z=149$ and $m/z=194$ correspond to intermediates after the
396 structure of the MB molecules broken into smaller molecules components. As shown in Fig. 5,
397 a possible degradation process is as follow. Firstly, Cl^- is ionized in aqueous solution, then the
398 loss of four $-CH_3$ connected to N proceeds, which has a smaller bond dissociation energy
399 (BDE) value in the MB molecular structure [23]. Secondly, the $-CH_3$ turns into HCHO or
400 $RCOO^-$. Thirdly, the C-S and C-N bonds in the middle ring which are the more active parts
401 are broken into other small molecular weight intermediates. Finally, all the organic
402 degradation products are transformed into CO_2 and H_2O , and these may contain inorganic
403 ions, such as Cl^- , SO_4^{2-} and NO_3^- in solution.

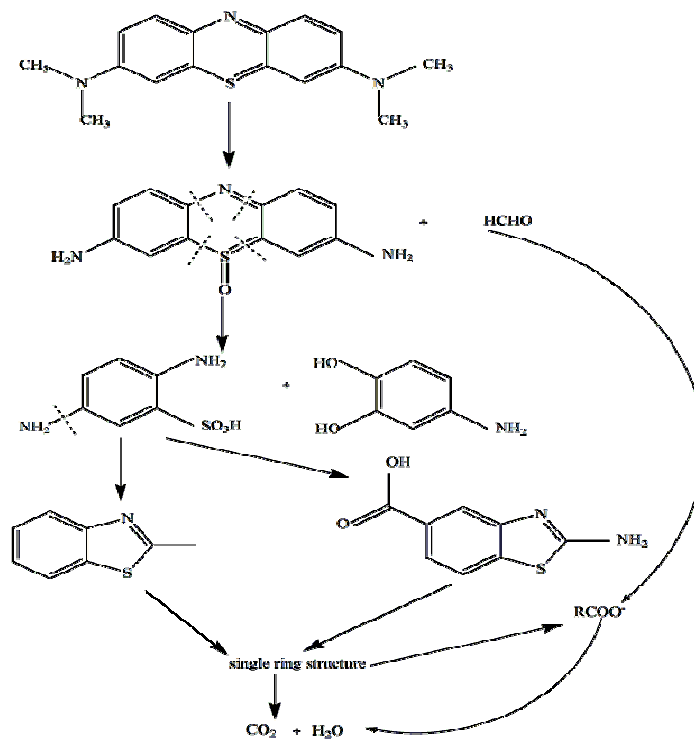
404



405

406 **Fig. 4.** Mass spectrometer of degraded products

407



408

409 **Fig.5.** The reduction degradation pathway of MB molecules

410

411 **4. Conclusions**

412 This study has demonstrated that green synthesis Fe NPs under various atmospheres (N₂, O₂
413 and air) can be used to remove MB due to its reduction by Fe⁰ nanoparticles and adsorption
414 on iron oxide nanoparticles. SEM and FTIR analyses showed that iron oxides were formed by
415 through the corrosion of Fe in oxygen and air atmosphere. Moreover, temperature had a
416 significant influence on the removal of MB. It indicated that the degradation process of MB
417 by N-Fe NPs, O-Fe NPs and air-Fe NPs was an endothermic reaction. The investigation of
418 kinetics demonstrated the degradation process of MB by N-Fe NPs fitted well to the pseudo-
419 second-order adsorption and pseudo-first-order reduction models. It was a chemisorption
420 process rather than a physical sorption one. While the degradation process of MB using O-Fe
421 NPs and air-Fe NPs seemed to fit well to pseudo-second-order adsorption and reduction
422 kinetics. Meanwhile, the Langmuir isotherm model proved that the degradation reaction had a
423 homogeneous and monolayer adsorption character. Finally, the degraded products obtained
424 from MB reacting with Fe NPs were identified by GC-MS analysis, and a possible
425 degradation pathway of MB using Fe NPs is proposed.

426 **Acknowledgement**

427 The authors thank the financial support given by the National Natural Science Foundation of
428 China (No. 41401585).

429 **References**

- 430 1. S. Dutta, A. Bhattacharyya, A. Ganguly, S. Gupta, B. Srabanti, *Desalination*. 2011, **275**,
431 26-36.
- 432 2. M. Iram, G. Chen, Y. P. Guan, A. Ishfaq, H. Z. Liu, *J. Hazard. Mater.* 2010, **181**, 1039-1050.
- 433 3. T. X. Wu, N. T. Li, J. C. Zhao, H. Hidaka, N. Serpone, *Environ Sci. Technol.* 1999, **33**

- 434 1379-1387.
- 435 4. A. Ghauch, A. Tuqan, H. A. Assi, *Environ. Pollut.* 2009, **157**, 1626-1635.
- 436 5. Y. M. Lin, Z. X. Chen, Z. L. Chen, M. Megharaj, R. Naidu, *Appl. Clay. Sci.* 2014, **93-94**,
- 437 56-61.
- 438 6. X. L. Weng, L. L. Huang, Z. L. Chen, M. Megharaj, R. Naidu, *Ind. Crops. Prod.* 2013, **51**,
- 439 342-347.
- 440 7. S. Iravani, *Green Chem.* 2011, **13**, 2638-2650.
- 441 8. L.L.Huang, X.L. Weng, Z.L.Chen, M.Megharaj, R.Naidu, *Spectrochim. Acta Part A* 2014,
- 442 **117**, 801-804.
- 443 9. Z. Q. Yu, S. S. C Chuang, *J. Phys. Chem. C.* 2007, **111**, 13813-13820.
- 444 10. Y. Bulut, H. Aydın, *Desalination*, 2006, **194**, 259-267.
- 445 11. F. L. Fu, D. D Dionysiou, H. Liu, *J. Hazard. Mater.* 2014, **267**, 194-205.
- 446 12. H. I. Chieng, T. Zehra, B. L. L Linda, *Environ. Earth. Sci.* 2014, **46**, 1-15.
- 447 13. D. Kavitha, C. Namasivayam, *Bioresour. Technol.* 2007, **98**, 14-21.
- 448 14. M. Auta, B. H. Hameed, *J. Eng. Chem.* 2011, **175**, 233-243.
- 449 15. P. Sharma, R. M. Das, *J. Chem. Eng.* 2013, **58**, 151-158.
- 450 16. A. Roy, B. Adhikari, S. B. Majumder, *Ind. Eng. Chem. Res.* 2013, **52**, 6502-6512.
- 451 17. M. Auta, B. H. Hameed, *J. Eng. Chem.* 2014, **237**, 352-361.
- 452 18. W. J. Jiang, C. Quan, X. Wei, *Environ. Sci. Technol.* 2014, **50**, 1-27.
- 453 19. W. Chen, D. Lin, D. Q. Zhu, *Environ. Sci. Technol.* 2007, **41**, 8295-8300.
- 454 20. S. Parimal, M. Prasad, U. Bhaskar, *Ind. Eng. Chem. Res.* 2010, **49**, 2882-2888
- 455 21. F. Tümsük, Ö. Avcı, *J. Eng. Chem.* 2013, **58**, 551-559.
- 456 22. Z. X. Chen, T. Wang, X. Y. Jin, Z. L. Chen, *J. Colloid Interface Sci.* 2013, **398**, 59-66.
- 457 23. F. M. Huang, C. Li, H. L. Wang, Z. C. Yan, *J. Eng. Chem. J.* 2010, **62**, 250-256.
- 458 24. B. Yang, J. N. Zuo, X. H. Tang, F. L. Liu, *Ultrason Sonochem.* 2014, **21**, 1310-1317.